Hindawi Publishing Corporation
International Journal of Photoenergy
Volume 2012, Article ID 453018, 9 pages
doi:10.1155/2012/453018

Research Article

Photocatalytical Properties and Theoretical Analysis of N, Cd-Codoped TiO_2 Synthesized by Thermal Decomposition Method

Hongtao Gao,[1,2] Bing Lu,[3] Fangfang Liu,[3] Yuanyuan Liu,[3] and Xian Zhao[1]

[1] *State Key Laboratory of Crystal Materials, Shandong University, Jinan 250100, China*
[2] *Department of Chemistry and Chemical Engineering, Jining University, Qufu 273155, China*
[3] *College of Chemistry and Molecular Engineering, Qingdao University of Science and Technology, Qingdao 266042, China*

Correspondence should be addressed to Hongtao Gao, gaohongtao@gmail.com

Received 19 June 2011; Revised 1 August 2011; Accepted 2 August 2011

Academic Editor: Jinlong Zhang

N, Cd-codoped TiO_2 have been synthesized by thermal decomposition method. The products were characterized by X-ray diffraction (XRD), scanning electron microscope (SEM), UV-visible diffuse reflectance spectra (DRS), X-ray photoelectron spectroscopy (XPS), and Brunauer-Emmett-Teller (BET) specific surface area analysis, respectively. The products represented good performance in photocatalytic degradation of methyl orange. The effect of the incorporation of N and Cd on electronic structure and optical properties of TiO_2 was studied by first-principle calculations on the basis of density functional theory (DFT). The impurity states, introduced by N 2p or Cd 5d, lied between the valence band and the conduction band. Due to dopants, the band gap of N, Cd-codoped TiO_2 became narrow. The electronic transition from the valence band to conduction band became easy, which could account for the observed photocatalytic performance of N, Cd-codoped TiO_2. The theoretical analysis might provide a probable reference for the experimentally element-doped TiO_2 synthesis.

1. Introduction

Due to its ability to decompose harmful organic pollutants completely [1, 2], nano-TiO_2 has attracted much interest in the last few decades as an environmental purification photocatalyst. However, the band gap of the TiO_2 is in the range of 3.0–3.2 eV (3.2 eV for anatase and 3.0 eV for rutile), and only the UV fraction of solar light (about 3–5%) is effective for inducing photoactivity [3]. It has been realized that doping played a dramatic role in shifting the absorption edge to a lower energy region and increasing the photocatalytic activity in the visible light region [4–7]. A substantial amount of research work have focused on improving the absorption of visible light (400–800 nm) by nonmetal doping with N [5, 7–9], C [4, 6, 10], S [11], F [12], I [13], B [14], P [15], and so forth.

Metal doping can significantly reduce the band gap and promote electronic excitation under visible light irradiation. Umebayashi et al. [16] reported that electron localization and migration by the dopant played an important role in light response of TiO_2. Mn-doping modified the electronic structure of rutile TiO_2 and improved the catalytic performance [17]. Andronic et al. [18] reported that there was a linear correlation between the band gap energy of the Cd-doped TiO_2 films and dyes photodegradation efficiency. Cd-doped mesoporous titania had high visible-light photocatalytic activities [19]. Whether as interstitial atom or lattice atom displacement, metal doping introduces impurity states between valance band (VB) and conduction band (CB), which act as electrons and holes recombination centers and can capture most of the charge carrier. So, the metal ion doping plays a limit role in improving the photocatalytic activity of TiO_2.

Due to doping, there always exist unfavorable factors, such as oxygen vacancy, brought by charge imbalance for either single metal or nonmetal element doping. However, the bielement doping is likely to maintain charge balance through charge compensation in the crystals. Wen et al. [20]

discussed the effect of bielement doping and the calcination temperature on the microstructure and photocatalytic activity of I, F codoped TiO_2. Nonionic surfactant was used as template to prepare N, F codoped TiO_2 for degradation of microcystin [21]. Xu et al. [22] found that there was a new electronic level in the structure of Ce, C codoped TiO_2 and pointed out that Ce doping could delay recombination of electrons and holes, shift the absorption to the red light region and enhance its photocatalytic activity. Tan et al. [23] studied the mechanism of light absorption and photocatalytic properties of Mo, N codoped TiO_2 and pointed out that oxygen vacancies played an important role in improving the photocatalytic performance of TiO_2. Due to the strong synergistic effect of W and N, the electronic structure was changed with the band gap narrowing and the optical absorption increasing [24]. Pingxiao et al. [25] studied preparation and photocatalysis of TiO_2 nanoparticles doped with nitrogen and cadmium, and the results of the study showed that nitrogen and cadmium codoping caused the absorption edge of TiO_2 to shift to the visible-light region. At present, the theoretical research of N, Cd-codoped anatase TiO_2 (101) surface has not been seen reported.

In our work, bare TiO_2, Cd-doped, N-doped and N, Cd-codoped TiO_2 photocatalysts have been synthesized by thermal decomposition method. The products were characterized by X-ray diffraction (XRD), scanning electron microscopy (SEM), UV-visible diffuse reflectance spectra (DRS), and X-ray photoelectron spectroscopy (XPS), respectively. The photocatalytic activities of samples were studied on the degradation of methyl orange (MO). First-principle calculations based on density functional theory (DFT) were performed to probe the effect of N and Cd incorporation on electronic structure and optical properties of TiO_2. To the best of our knowledge, this is the first theoretical explanation to rationalize the gap narrowing mechanism and the substitutional and adsorptive roles of N and Cd doping in surface-state anatase. The theoretical calculations were used to account for the experimental observation which was high photocatalytic performance of N, Cd-codoped TiO_2 for organic pollutants degradation.

2. Experimental

2.1. Photocatalyst Preparation. The photocatalyst series have been synthesized by thermal decomposition method, using dodecylamine as nitrogen source and cadmium nitrate ($Cd(NO_3)_2$) as Cadmium source. Isopropanol and tetra-n-butyl titanate (TTNB) were added into 250 mL round-bottom flask in turn according to a certain proportion, then 100 mL acetic acid solution (pH = 2) was added with magnetic stirring to form transparent solution. After then, dodecylamine and Cd $(NO_3)_2$ was added into the solution according to certain molar ratio. The obtained solution was then transferred to a 250 mL three-neck boiling flask. After having been stirred vigorously for 24 h, it was heated in the paraffin bath, with the temperature rising gradually to 120°C at a rate of 10°C/h and temperature heating for two hours, until a white precipitate appeared. The precipitate was washed with ethanol until pH = 7 and dried at 60°C for 24 hours, forming a white solid composite. Finally, the samples were calcined at certain temperature in muffle furnace for 2 hours. Bare TiO_2, Cd-doped TiO_2, and N-doped TiO_2 were prepared in the same way.

2.2. Characterization. The crystalline phase of the powders that evolved after calcination was examined by XRD with a Rigaku D/MAX-2000 diffractometer, using Cu Kα irradiation ($\lambda = 0.154056$ nm) at 45 kV and 40 mA. The crystallite size (D) was estimated from the width of lines in the XRD pattern according to the Scherrer equation. A scanning electron microscope (SEM) JSM-6300 (JEOL Ltd, Japan) was used to investigate the surface morphology of the sample. In addition, UV-vis diffuse spectra were measured at room temperature with a UV-vis spectrometer (Cary-500, Varian Co.). Nitrogen adsorption-desorption isotherms at 77 K were measured using a Quantacherome Nove 1000e system, and the Brunauer-Emmett-Teller (BET) surface area was calculated from the linear part of BET plot. X-ray photoelectron spectroscopy (XPS) measurements were performed with the ESCALAB 250 Microprobe System (ThermoFisher SCIENTIFIC), using the Mg K Line of a 300 W Mg X-ray tube as a radiation source at 15 kV. All the binding energies were referenced to the C 1s peak at 284.8 eV of the surface adventitious carbon.

2.3. Photocatalytic Activity Measurements. Photocatalytic activity of photocatalysts was evaluated by the degradation of MO, which was performed in an SGY-I photochemical reactor (Nanjing, Stonetech. EEC Ltd. Nanjing, China). A quartz cylinder (50×450 mm) was placed inside the reactor and illuminated with 300 W high-pressure mercury lamp. For each condition, a certain amount of powders was added into 500 mL of aqueous solution of MO (20 mg·L^{-1}). A magnetic stirrer was located at the bottom of the quartz cylinder so that a homogeneous TiO_2 suspension could be maintained throughout the reaction. The solutions containing photocatalysts were stirred mechanically in the dark for 30 min to ensure adsorption-desorption equilibrium between MO and photocatalyst powders. The photocatalytic experiment was repeated under the identical reaction conditions to confirm the reproducibility. During the experimental process, 5 mL of aqueous suspension was taken from the quartz cylinder after specific intervals, centrifuged, and filtered through 0.45 μm millipore filter to monitor the degradation of MO dye. UV spectrophotometer (UV-vis Cary50; Varian Co.) was used to monitor changes in the spectral intensity distribution of the dye.

3. Results and Discussions

3.1. XRD Analysis. The phase structure, crystallite size, and crystallinity of TiO_2 play an important role in photocatalytic activity, and many studies have confirmed that anatase phase of titania shows higher photocatalytic activity than brookite or rutile phase [26]. The XRD patterns of TiO_2 photocatalysts calcined at 450°C were showed in Figure 1. There existed sharp diffraction peaks, which lay at 25.4°, 37.9°, 48.0° and 53.9°, corresponding to (101), (004),

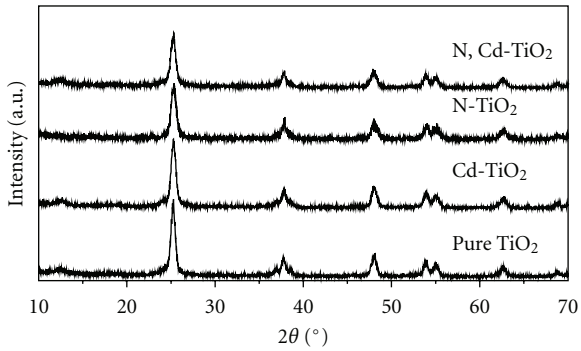

Figure 1: XRD patterns of photocatalysts calcined at 450°C.

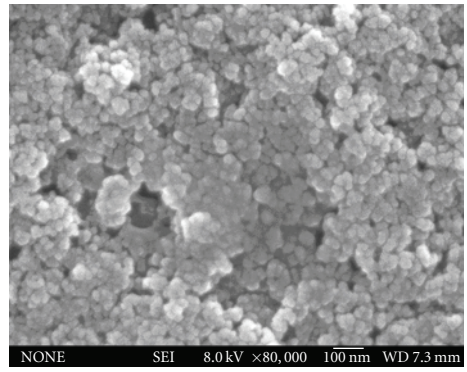

Figure 2: SEM images of N, Cd-codoped TiO_2 calcined at 450°C.

(200), (105) anatase crystal plane diffraction, respectively. There were no apparent diffraction peaks at 27.5° and 54.5° in the XRD patterns, indicating the rutile phase did not exist in the sample. It indicated that the prepared products were anatase-TiO_2 monophase and element-doping did not affect the crystalline phase of TiO_2 catalyst.

It was also seen in Figure 1 that the intensity of the maximum diffraction peak ($2\theta = 25.4°$) of the bare TiO_2, Cd-TiO_2, N-TiO_2, and N, Cd-codoped TiO_2 decreased in turn. The average size of crystallites was estimated based on the broadening of (101) peak at $2\theta = 25.4°$ according to Scherrer equation. The crystal diameter of bare TiO_2, Cd-TiO_2, N-TiO_2 and N, Cd-TiO_2 was 14.56 nm, 12.55 nm, 13.34 nm, and 12.60 nm, respectively. It indicated that element-doping inhabited the crystal grain growth and particles aggregation, resulting in larger specific area. Small particle size could shorten the route of an electron migrates from the conduction band of the TiO_2 to its surface, while large surface area could provide more active sites and absorb more reactive species. Additionally, there was no new crystalline phase for Cd-TiO_2, N-TiO_2, and N, Cd-TiO_2, illustrating that the N and Cd doping did not change the catalysts phase.

3.2. SEM Analysis. Figure 2 showed SEM micrograph of the calcinated samples at 450°C. The SEM images showed that nanoparticles were uniform (12~15 nm), global and slightly agglomerated. Further observation indicated that the morphology of samples was very rough and might be beneficial to enhancing the adsorption of reactants.

3.3. UV-Vis DRS Analysis. Figure 3 illustrated the UV-vis DRS of the photocatalysts. Compared to the strong absorption in the UV region, the absorption in the visible region was relatively weak for all the photocatalysts. Both in the UV region (<400 nm) and visible region, the absorptions of as-prepared photocatalysts were all stronger than that of pure TiO_2. The intensity of absorption of pure TiO_2, Cd-TiO_2, N-TiO_2, and N, Cd-doped TiO_2 increased in turn, and the absorption intensity of N, Cd-codoped TiO_2 was the strongest. The band gap (E_g) of the photocatalysts could be calculated for practical purposes by the following equation [27]

$$E_g = \frac{1240}{\lambda}, \quad (1)$$

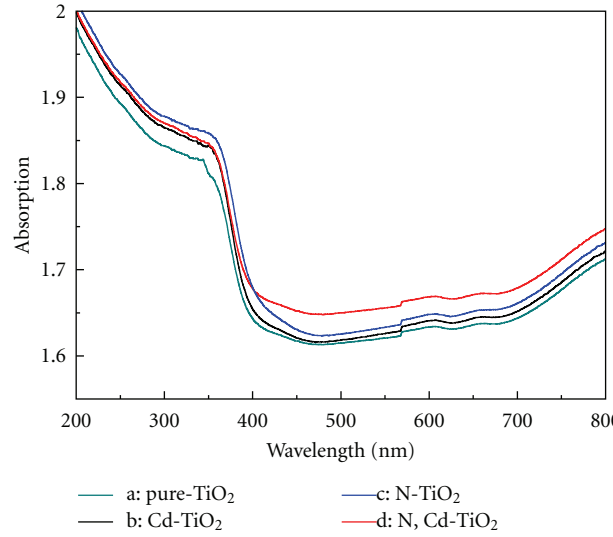

Figure 3: DRS of photocatalysts: a: pure TiO_2, b: Cd-doped TiO_2, c: N-doped TiO_2, and d: N, Cd-codoped TiO_2.

where λ is the absorbance wavelength. The band gaps of TiO_2 catalysts were shown in Table 1. The E_g of pure TiO_2, Cd-codoped, N-doped, and N, Cd-codoped TiO_2 was 3.20 eV, 3.16 eV 3.15 eV, and 3.08 eV, respectively. The band gaps of as-prepared photocatalysts were all smaller than that of pure TiO_2. The absorption edges of Cd-doped TiO_2 (392.4 nm), N-doped TiO_2 (394 nm), and N, Cd-codoped TiO_2 (402.6 nm) were larger than that of pure TiO_2 (387.5 nm), which indicated that the observation of optical bands in the visible range (400–550 nm) could be ascribed to doping. The absorption in the visible region might be induced by a subband-gap transition corresponding to the excitation from the valence band to the impurity band [9]. The absorption of N, Cd-codoped TiO_2 in the visible light (λ = 402.6 nm) was the maximum, indicating the codoping of N and Cd might have a synergistic effect on enhancing the photocatalytic activity.

3.4. Surface Area Analysis. The photocatalytic activity of photocatalyst is relative to the number of active surface sites, the surface properties of photocatalysts often have

Table 1: Absorption edges and the band gaps of samples.

	Pure TiO_2	Cd-TiO_2	N-TiO_2	N, Cd-TiO_2
λ (nm)	387.5	392.4	394	402.6
E_g (eV)	3.20	3.16	3.15	3.08

important effects on their photocatalytic activity. The BET surface area of N, Cd-TiO_2 (102.67 m^2/g) was also higher than those of Cd-TiO_2 (95.63 m^2/g), N-TiO_2 (81.90 m^2/g), and bare TiO_2 (69.81 m^2/g). It could be concluded from the experimental results that element-doping inhabited the crystal grain growth and particles aggregation. And the addition of N and Cd played the synergistic effect in modification the structure of TiO_2. The doping led to the crystal structure distortion, crystallinity reduction, and the specific surface area increasing, which would enhance the effective organic adsorption on the surface of catalyst. It also made the electronic migration from crystal inner to surface easy. The crystal surface defects could inhibit the electron-hole pairs on the catalyst surface, which would result in the photocatalytic activity increasing. It also indicated that the strong synergistic interaction of N and Cd appeared to play an important role in driving the excellent photoactivity performance of the N, Cd-TiO_2, which could be seen in Section 3.6.

3.5. XPS Analysis. The XPS survey spectrum of the N, Cd-TiO_2 was showed in Figure 4(a). XPS peaks showed that the N, Cd-TiO_2 photocatalyst contained Ti, O, N, and Cd elements and a trace amount of carbon. The presence of carbon was ascribed to the residual carbon from the precursor solution and the adventitious hydrocarbon from the XPS instrument itself.

Figure 4(b) showed the N1s XPS spectrum of the N, Cd-codoped TiO_2. A peak appeared at 405.4 eV and a small peak appeared at 399.6 eV, which was ascribed to the N atoms from adventitious N–N, N–H, O–N, or N-containing organic compounds adsorbed on the surface of TiO_2 [5]. This analysis indicated that N atoms were incorporated into the TiO_2 crystallattice under our experimental condition. Figure 4(c) showed the Cd 3d XPS spectra of N, Cd-TiO_2. A peak appeared at 405.3 eV and was ascribed to the Cd atoms (Cd 3d5/2) from Cd and $CdCO_3$. The results showed that Cd did not incorporate into the TiO_2 crystal lattice but existed in the form of $CdCO_3$. It might also suggest that Cd was gradually excluded from the Ti-O framework to the surface of titania, and hindered the anatase crystallites from growing in size.

3.6. Photocatalytic Activity. Figure 5 showed the relationship between the degradation and the irradiation time for each photocatalyst during the photocatalytic degradation of MO. It indicated that there were obvious photocatalytic activities under irradiation for all photocatalysts. Until irradiated for 15 minutes, the degradation rates on the MO for bare TiO_2, Cd-TiO_2, N-TiO_2, N, Cd-codoped TiO_2 were 88%, 95%, 97%, and 99%, respectively. And the degradation rate corresponding to the N, Cd-codoped TiO_2 catalyst was the highest. After being irradiated for no more than 30 minutes, the degradation rates of as-prepared photocatalysts all almost reached 100% (pure TiO_2, Cd-TiO_2 N-TiO_2, N, Cd-codoped TiO_2 were 99.0%, 99.3%, 99.4%, and 99.6%, resp.). The enhanced photocatalytic performance showed N, Cd codoping played a synergistic role in the improvement of the photocatalytic properties of titania. It indicated that element codoping was an effective means to improve the photocatalytic performance of photocatalysts.

4. Theoretical Analysis

4.1. Calculation Models and Methods. First-principles calculation based on DFT [28, 29] was performed to explore the effect of dopants on the electronic structure and optical properties of photocatalysts. The anatase (101) surface was modeled with a periodically repeated slab. We considered a pure TiO_2 surface supercell containing 96 atoms, of dimension 2×2 in the [101] and [010] directions, respectively, corresponding to a surface area of 10.89×7.55 Å^2 and the number of the atom layers was 4. It was named as $2 \times 2 - 4$, as shown in Figure 6(a). The other model was created based on it. To ensure interaction between the upper and lower layers be ignored, the vacuum thickness was set to 10 Å. According to the experimental XPS results, one kind of defect surface was considered, namely, substitutional N, adsorptive Cd model ($Ti_{32}CdO_{63}N$). The supercell of $Ti_{32}CdO_{63}N$ was shown in Figure 6(b). Side view of (a) the four-layer relaxed slab, which was used in surface properties calculations and labeled $Ti_{32}O_{64}$, (b) $Ti_{32}CdO_{63}N$ was simulated by replacing one oxygen atom with nitrogen atom and adding one cadmium atom on the surface of the supercell.

The calculations in our work have been carried out using the well-tested CASTEP code [30, 31], which employs planewave basis sets to treat valence electrons and pseudopotentials to approximate the potential field of ionic cores (including nuclei and tightly bond core electrons). The general gradient approximation (GGA) with PW91 functional [32] and ultrasoft pseudopotentials [33] were used to describe the exchange-correlation effects and electron-ion interactions, respectively. N (2s2 2p3), O (2s2 2p4), Ti (3s2 3p6 3d2 4s2), and Cd (4d10 5s2) electrons were considered as valence states, while the remaining electrons were kept frozen as core states. Pulay density hybrid method was used in energy calculations, convergence threshold for self-consistent field was set to 2.0×10^{-6} eV/atom. The k-point sampling of the Brillouin zone was set to $2 \times 3 \times 1$. Fast Fourier change for $50 \times 40 \times 120$. The Broyden-Fletcher-Goldfarb-Shanno (BFGS) algorithm has been used for geometry optimizations and the atomic relaxation was carried out until all components of the residual forces were less than 0.05 eV/Å, the energy and the displacement tolerances were set to 2.0×10^{-5} eV/atom and 2×10^{-3} nm, respectively. In calculation, the geometry models of TiO_2 supercell were optimized firstly, then their electronic structures and optical properties were calculated. All the calculations were performed in the reciprocal space.

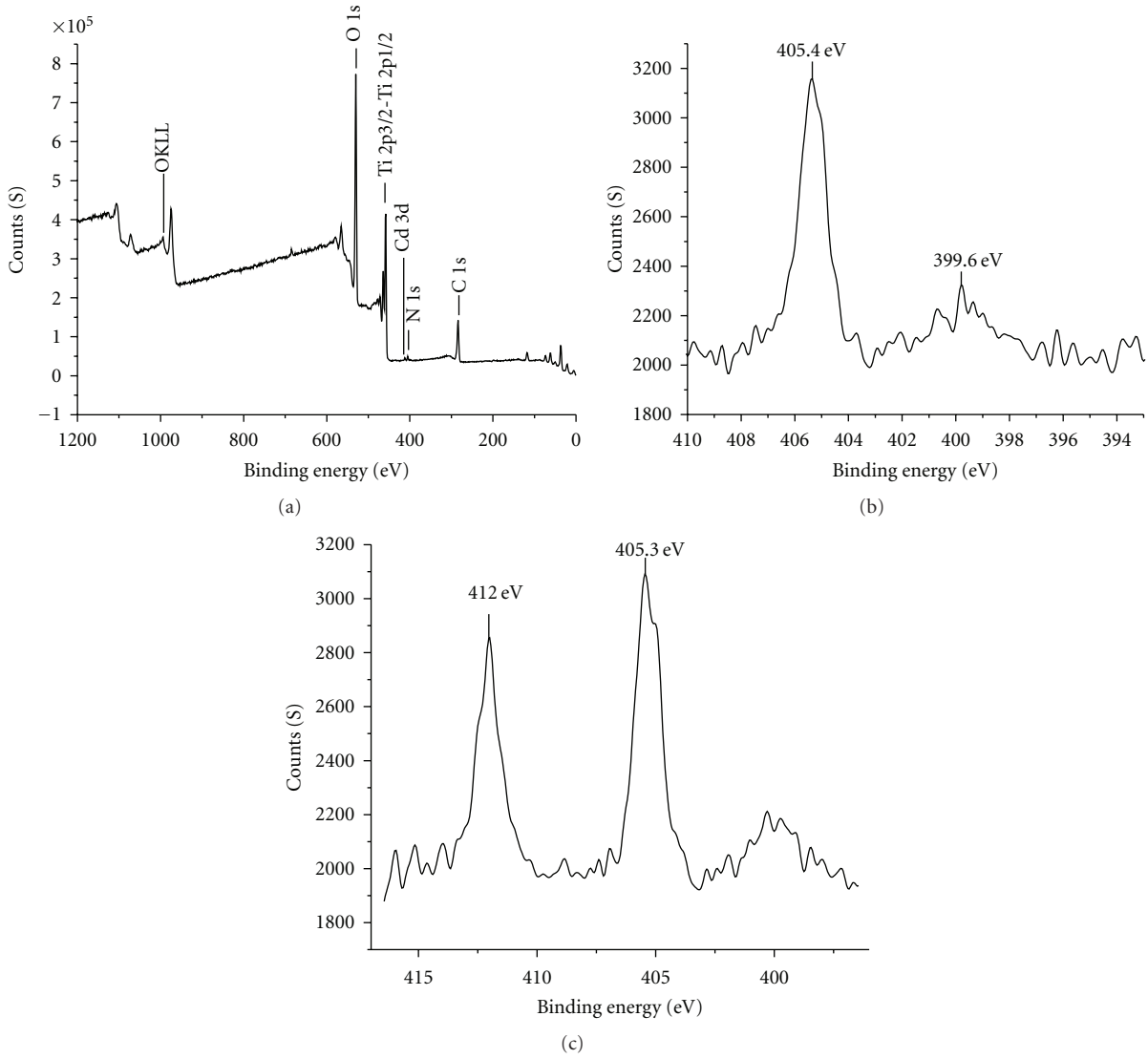

Figure 4: (a) The survey XPS spectra of N, Cd-TiO_2, (b) N 1s XPS spectra of N, Cd-TiO_2, (c) Cd 3d XPS spectra of N, Cd-TiO_2.

4.2. Results and Discussions

4.2.1. Impurity Formation Energy and Structural Optimization. By optimizing the pure anatase TiO_2 unit cell, the unit cell parameters were obtained as follows: $a = b = 3.8174$ Å, $c = 9.6950$ Å, dap = 2.0050 Å, deq = 1.9540 Å, and $2\theta = 155.917°$. They were in good agreement with experimental results [34]: $a = b = 3.7848$ Å, $c = 9.5124$ Å, dap = 1.9799 Å, deq = 1.9338 Å, and $2\theta = 156.230°$. This result implied that our calculations were reliable and believable.

In order to determine the stabilities of the doped systems, we calculated the formation energies (E_f) of the doped systems according to the following formula (1)

$$E_f = E_{TiO_2:D} + \frac{1}{2}E_{O_2} + nE_{Ti} - E_{TiO_2} - \frac{1}{2}E_{N_2} - E_{Cd}, \quad (2)$$

where $E_{TiO_2:D}$ and E_{TiO_2} were the total energy of N, Cd codoped TiO_2, pure TiO_2 in the same size supercells. E_{N_2} and E_{O_2} were the energy of N_2 and O_2 gas molecular, E_{Cd} and E_{Ti} were the energy of bulk Cd and Ti metal, respectively, n was the number of titanium atoms replaced by Cadmium atoms in the doping system. The calculated results was shown in Table 2. According to the results, we discovered that the E_f of $Ti_{32}CdO_{63}N$ was positive, which indicated that the synthesis of N, Cd codoped TiO_2 required energy.

The crystal data of pure and N, Cd codoped TiO_2 were shown in Table 2 In $Ti_{32}CdO_{63}N$, the Ti–O bond length 1.9585 Å was longer than the original Ti–O one 1.9543 Å. The Ti–N bond length 1.8976 Å was shorter than the Ti–O calculated value 1.9585 Å, due to the smaller radius of N compared to O^{2-} The changes of O–Ti–O(N) bond angle in $Ti_{32}CdO_{63}$ N were noticeable compared to pure TiO_2. All these factors could lead to higher dipole moments in TiO6 octahedron. Sato et al. [35] found that the local internal fields due to the dipole moment of distorted octahedral promote the charge separation in the very initial process of

Table 2: Formation energies and optimized structural parameters for pure and N, Cd codoped TiO_2.

	E_f (eV)	Bond length (Å)		O–Ti–O(N) bond angle (°)	
		Ti–O	Ti–N	—	
Pure TiO_2	—	1.9543	—	160.503	102.154
$Ti_{32}CdO_{63}N$	3.630	1.9585	1.8976	163.055	90.353

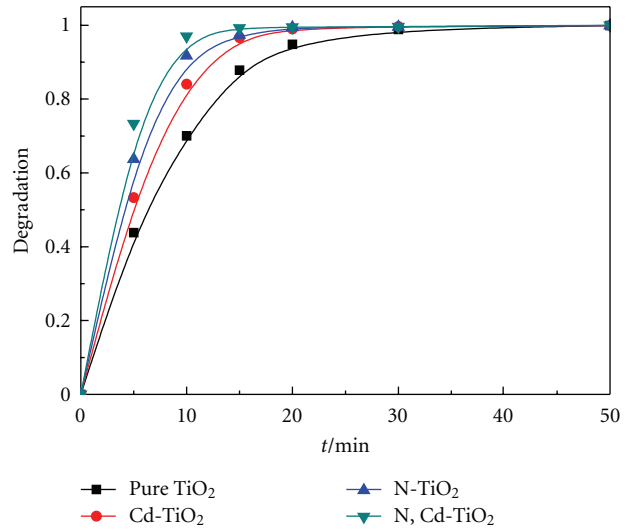

Figure 5: Photocatalytic degradation of MO by photocatalysts.

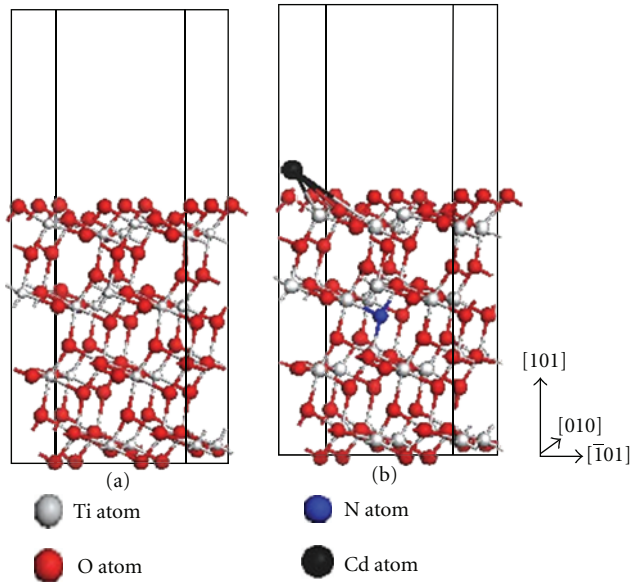

Figure 6: The model of supercells: (a) $Ti_{32}O_{64}$, (b) $Ti_{32}CdO_{63}N$.

photoexcitation. The electron-hole pair can separate more easily and recombine slower, and the photocatalysts show a better photocatalytic performance. This was one reason for N, Cd codoped TiO_2 showed a higher activity.

4.2.2. Electronic Structure Analysis. To investigate the effect of dopants on the electronic structure and properties of TiO_2, the band structure and the partial density of states (PDOS) of the anatase TiO_2 were calculated. The band structure for the bare TiO_2 was showed in Figure 7(a) with the Fermi energy being 0 eV on the energy axis. And the PDOS for the bare TiO_2 was presented in Figure 7(b). The PDOS for the bare TiO_2 revealed that the bottom of conduction bands (CB) was mostly composed of Ti 3d states and the top of valence bands (VB) was dominated by O 2p states, which can be seen in Figure 7(b). It was showed in Figure 7(a) that the valence band maximum (VBM) and the conduction band minimum (CBM) located at G point, which indicated that bare TiO_2 was a direct-gap semiconductor material. The minimum gap between VBM and CBM (E_g) was 2.458 eV, which was lower than the experimental value of 3.20 eV. This underestimation of the energy gap was mainly due to the well-known shortcoming of the exchange-correlation functional in describing excited states [36]. However, as a kind of effective approximation, its relative calculation value was quite exact, and it did not affect theoretical analysis on electronic structure analysis.

The band structure and PDOS of N, Cd-TiO_2 ($Ti_{32}CdO_{63}N$, substitutional N, adsorptive Cd) were presented in Figures 8(a) and 8(b), respectively. The band structure of TiO_2 was modified by N and Cd codoping. The PDOS for the N, Cd-TiO_2 revealed that the conduction band consisted of the Ti 3d states mainly, and the valence bands (VB) was dominated by O 2p, Ti 3d, and Cd 4d states, which can be seen in Figure 8(b). As showed in Figure 8(a), there were two kinds of impurity states, which came from N 2p and Cd 5s, respectively, between valence bands and conduction bands. The impurity state from Cd 5s lied 0.655 eV below the bottom of the conduction band, which could absorb smaller photon energy and achieved indirect transition so that the light absorption of TiO_2 extended to the visible light area. While the impurity state from N 2p lied 0.244 eV above the top of the valence band, which made it become a shallow acceptor level.

Since the shallow acceptor would be act as capture trap for photoexcited electrons, the impurity states between VBM and CBM could reduce the recombination rate of photoexcited carriers, which were very crucial for the enhancement of the photocatalysis efficiency. Compared to bare TiO_2, both CBM and VBM of $Ti_{32}CdO_{63}N$ shifted to the low energy level, which indicated that $Ti_{32}CdO_{63}N$ had stronger redox ability than bare TiO_2. The energy gap narrowed from 2.458 eV to 2.225 eV, which made the electron transiting from valence band to conduction band become easy. All the above results implied that nitrogen and cadmium codoping resulted in red shift of the optical absorption edge and could greatly enhance the photocatalytic activity of TiO_2. It was

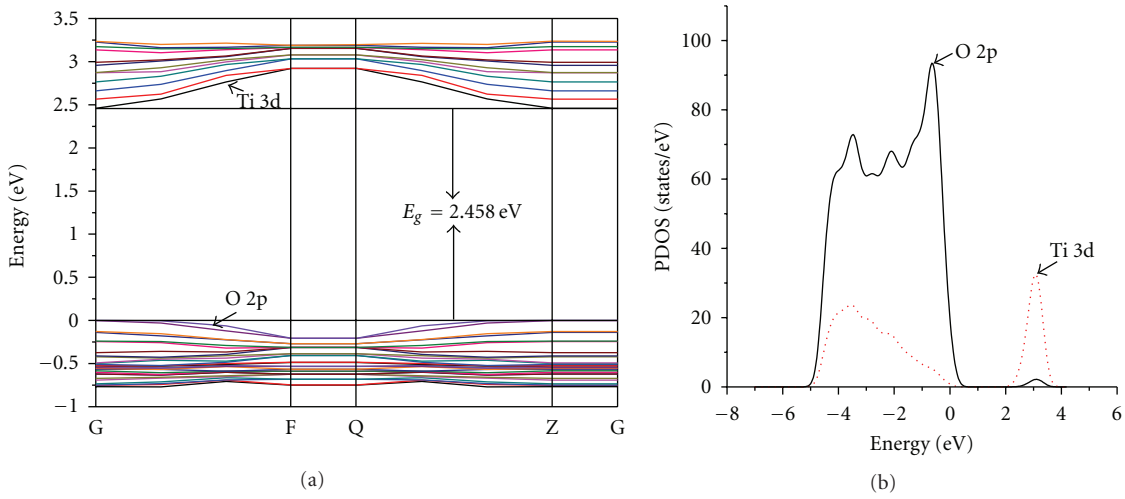

Figure 7: $Ti_{32}O_{64}$: (a) band structure, (b) partial density of state.

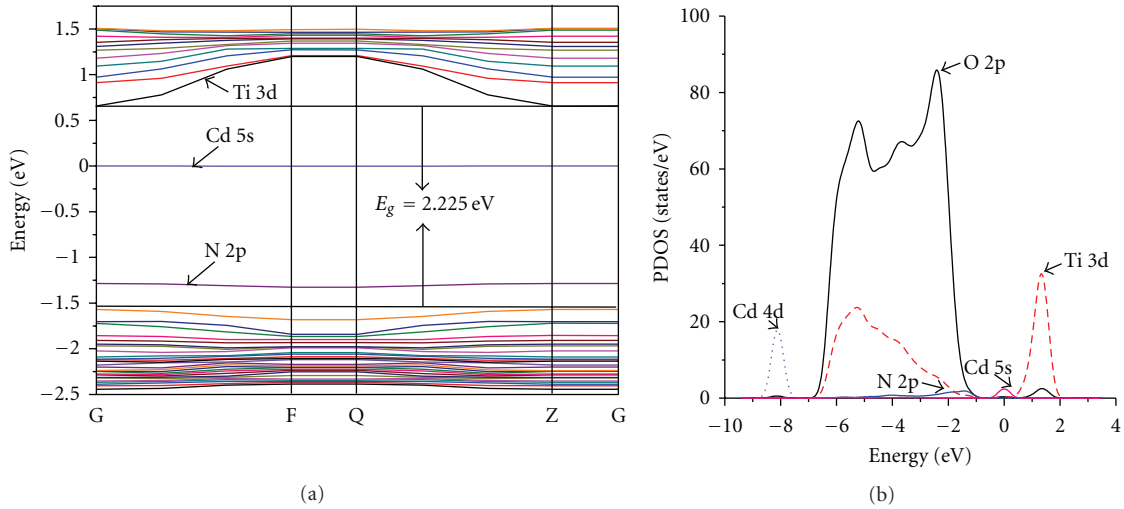

Figure 8: $Ti_{32}CdO_{63}N$: (a) band structure, (b) partial density of state.

consistent with the experimentally observed absorption of N, Cd-TiO_2 in the visible region.

4.2.3. Optical Properties. In order to make the calculated results more correspond with the actual situation, in the calculation of the optical properties using the "scissor operators" fixed: 0.742 eV (the difference between band gap of measured and calculated). Photo absorption coefficient were calculated with function polycrystalline and using the photo wavelength as the horizontal axis, the optical absorption coefficient as the vertical axis in this paper. The calculated optical absorption spectrum diagram was shown in Figure 9. It was showed in Figure 9 that the absorption coefficient of N, Cd-TiO_2 were higher than that of the bare TiO_2 in the wavelength region from 350 nm to 780 nm, and the optical absorption edge shifted to long-wavelength range. The optical characteristics corresponded to their electronic structures, modified by N and Cd codoping with the energy gap reduction and introduction of impurity states between the VBM and CBM. Theoretical calculation results could account for the experimental observation.

5. Conclusions

Bare TiO_2, Cd-doped, N-doped, and N, Cd-codoped TiO_2 photocatalysts have been synthesized by thermal decomposition. The photocatalysts possessed an anatase crystalline framework having particle sizes of 10–15 nm. The corresponding absorption edge was 387.5 nm, 392.4 nm, 394.0 nm, and 402.6 nm, respectively, which indicated they represented photocatalytic activities in the visible region. N atoms were incorporated into the crystallattice, while Cd atoms existed on the crystal surface of TiO_2. The codoping of N and Cd might have a synergistic effect on enhancing the photocatalytic activity of TiO_2. The first-principle calculations indicated the energy gap of N, Cd-codoped

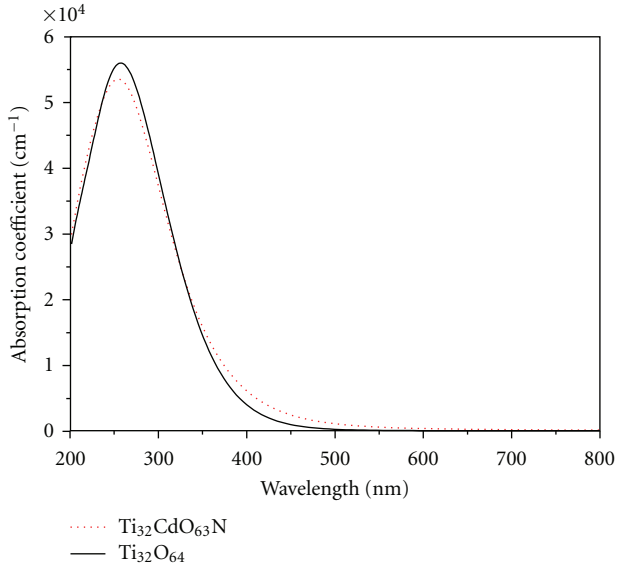

Figure 9: Absorption spectra of the pure and N, Cd-codoped anatase TiO_2.

TiO_2 became narrow and local internal fields of codoping enabled photoexcited electron-hole pair's separation became very easy. Excitation from the impurity states of N 2p or Cd 5s to the conduction band could account for the optical absorption edge shifted toward the low energy level, which was consistent with the experimentally observation. N, Cd-codoped TiO_2 perform better photocatalytic activity in the visible light region than the bare TiO_2. The theoretical analysis might provide a probable reference for the experimental synthesis of new photocatalysts in the future.

Acknowledgments

This work has been cosupported by the Outstanding Adult-Young Scientific Research Encouraging Foundation of Shandong Province (Grant no. 2008BS09016) and the Scientific Research Program of Shandong Province Education Department (Grant no. J08LC55).

References

[1] A. Fujishima and K. Honda, "Electrochemical photolysis of water at a semiconductor electrode," *Nature*, vol. 238, no. 5358, pp. 37–38, 1972.

[2] K. Dai, T. Peng, H. Chen, R. Zhang, and Y. Zhang, "Photocatalytic degradation and mineralization of commercial methamidophos in aqueous titania suspension," *Environmental Science and Technology*, vol. 42, no. 5, pp. 1505–1510, 2008.

[3] T. C. Jagadale, S. P. Takale, R. S. Sonawane et al., "N-doped TiO_2 nanoparticle based visible light photocatalyst by modified peroxide sol-gel method," *Journal of Physical Chemistry C*, vol. 112, no. 37, pp. 14595–14602, 2008.

[4] S. U. M. Khan, M. Al-Shahry, and W. B. Ingler, "Efficient photochemical water splitting by a chemically modified n-TiO_2," *Science*, vol. 297, no. 5590, pp. 2243–2245, 2002.

[5] R. Asahi, T. Morikawa, T. Ohwaki, K. Aoki, and Y. Taga, "Visible-light photocatalysis in nitrogen-doped titanium oxides," *Science*, vol. 293, no. 5528, pp. 269–271, 2001.

[6] F. Dong, H. Wang, and Z. Wu, "One-step "Green" synthetic approach for mesoporous C-doped titanium dioxide with efficient visible light photocatalytic activity," *Journal of Physical Chemistry C*, vol. 113, no. 38, pp. 16717–16723, 2009.

[7] X. Qiu and C. Burda, "Chemically synthesized nitrogen-doped metal oxide nanoparticles," *Chemical Physics*, vol. 339, no. 1–3, pp. 1–10, 2007.

[8] X. Li, H. Wang, J. T. Robinson, H. Sanchez, G. Diankov, and H. Dai, "Simultaneous nitrogen doping and reduction of graphene oxide," *Journal of the American Chemical Society*, vol. 131, no. 43, pp. 15939–15944, 2009.

[9] H. Gao, J. Zhou, D. Dai, and Y. Qu, "Photocatalytic activity and electronic structure analysis of N-doped anatase TiO_2: a combined experimental and theoretical study," *Chemical Engineering and Technology*, vol. 32, no. 6, pp. 867–872, 2009.

[10] H. Gao, C. Ding, and D. Dai, "Density functional characterization of C-doped anatase TiO_2 with different oxidation state," *Journal of Molecular Structure*, vol. 944, no. 1–3, pp. 156–162, 2010.

[11] F. Tian and C. Liu, "DFT description on electronic structure and optical absorption properties of anionic S-doped anatase TiO_2," *Journal of Physical Chemistry B*, vol. 110, no. 36, pp. 17866–17871, 2006.

[12] J. K. Zhou, L. Lv, J. Yu et al., "Synthesis of self-organized polycrystalline F-doped TiO_2 hollow microspheres and their photocatalytic activity under visible light," *Journal of Physical Chemistry C*, vol. 112, no. 14, pp. 5316–5321, 2008.

[13] W. Su, Y. Zhang, Z. Li et al., "Multivalency iodine doped TiO_2: preparation, characterization, theoretical studies, and visible-light photocatalysis," *Langmuir*, vol. 24, no. 7, pp. 3422–3428, 2008.

[14] S. In, A. Orlov, R. Berg et al., "Effective visible light-activated B-doped and B,N-codoped TiO_2 photocatalysts," *Journal of the American Chemical Society*, vol. 129, no. 45, pp. 13790–13791, 2007.

[15] F. Li, Y. Jiang, M. Xia et al., "Effect of the P/Ti ratio on the visible-light photocatalytic activity of P-doped TiO_2," *Journal of Physical Chemistry C*, vol. 113, no. 42, pp. 18134–18141, 2009.

[16] T. Umebayashi, T. Yamaki, H. Itoh, and K. Asai, "Analysis of electronic structures of 3d transition metal-doped TiO_2 based on band calculations," *Journal of Physics and Chemistry of Solids*, vol. 63, no. 10, pp. 1909–1920, 2002.

[17] G. Shao, "Electronic structures of manganese-doped rutile TiO_2 from first principles," *Journal of Physical Chemistry C*, vol. 112, no. 47, pp. 18677–18685, 2008.

[18] L. Andronic, A. Enesca, C. Vladuta, and A. Duta, "Photocatalytic activity of cadmium doped TiO_2 films for photocatalytic degradation of dyes," *Chemical Engineering Journal*, vol. 152, no. 1, pp. 64–71, 2009.

[19] H. Y. Hao, C. X. He, B. Z. Tian, and J. L. Zhang, "Study of photocatalytic activity of Cd-doped mesoporous nanocrystalline TiO_2 prepared at low temperature," *Research on Chemical Intermediates*, vol. 35, no. 6-7, pp. 705–715, 2009.

[20] C. Wen, Y. J. Zhu, T. Kanbara, H. Z. Zhu, and C. F. Xiao, "Effects of I and F codoped TiO_2 on the photocatalytic degradation of methylene blue," *Desalination*, vol. 249, no. 2, pp. 621–625, 2009.

[21] M. Pelaez, A. A. de la Cruz, E. Stathatos, P. Falaras, and D. D. Dionysiou, "Visible light-activated N-F-codoped TiO_2 nanoparticles for the photocatalytic degradation of microcystin-LR in water," *Catalysis Today*, vol. 144, no. 1-2, pp. 19–25, 2009.

[22] J. Xu, Y. Ao, and D. Fu, "A novel Ce, C-codoped TiO_2 nanoparticles and its photocatalytic activity under visible light," *Applied Surface Science*, vol. 256, no. 3, pp. 884–888, 2009.

[23] K. Tan, H. Zhang, C. Xie, H. Zheng, Y. Gu, and W. F. Zhang, "Visible-light absorption and photocatalytic activity in molybdenum- and nitrogen-codoped TiO_2," *Catalysis Communications*, vol. 11, no. 5, pp. 331–335, 2010.

[24] A. Kubacka, G. Colón, and M. Fernández-García, "N- and/or W-(co)doped TiO_2-anatase catalysts: effect of the calcination treatment on photoactivity," *Applied Catalysis B*, vol. 95, no. 3-4, pp. 238–244, 2010.

[25] W. Pingxiao, T. Jianwen, and D. Zhi, "Preparation and photocatalysis of TiO_2 nanoparticles doped with nitrogen and cadmium," *Materials Chemistry and Physics*, vol. 103, no. 2-3, pp. 264–269, 2007.

[26] O. Carp, C. L. Huisman, and A. Reller, "Photoinduced reactivity of titanium dioxide," *Progress in Solid State Chemistry*, vol. 32, no. 1-2, pp. 33–177, 2004.

[27] T. Lopez, R. Gomez, E. Sanchez, F. Tzompantzi, and L. Vera, "Photocatalytic activity in the 2,4-dinitroaniline decomposition over TiO_2 sol-gel derived catalysts," *Journal of Sol-Gel Science and Technology*, vol. 22, no. 1-2, pp. 99–107, 2001.

[28] J. Taylor, H. Guo, and J. Wang, "Ab initio modeling of quantum transport properties of molecular electronic devices," *Physical Review B*, vol. 63, no. 24, Article ID 245407, pp. 2454071–24540713, 2001.

[29] K. Yang, Y. Dai, B. Huang, and M. H. Whangbo, "Density functional characterization of the band edges, the band gap states, and the preferred doping sites of halogen-doped TiO_2," *Chemistry of Materials*, vol. 20, no. 20, pp. 6528–6534, 2008.

[30] H. Kamisaka, T. Adachi, and K. Yamashita, "Theoretical study of the structure and optical properties of carbon-doped rutile and anatase titanium oxides," *Journal of Chemical Physics*, vol. 123, no. 8, Article ID 084704, 9 pages, 2005.

[31] C. Di Valentin, G. Pacchioni, A. Selloni, S. Livraghi, and E. Giamello, "Characterization of paramagnetic species in N-doped TiO_2 powders by EPR spectroscopy and DFT calculations," *Journal of Physical Chemistry B*, vol. 109, no. 23, pp. 11414–11419, 2005.

[32] J. P. Perdew and Y. Wang, "Accurate and simple analytic representation of the electron-gas correlation energy," *Physical Review B*, vol. 45, no. 23, pp. 13244–13249, 1992.

[33] D. Vanderbilt, "Soft self-consistent pseudopotentials in a generalized eigenvalue formalism," *Physical Review B*, vol. 41, no. 11, pp. 7892–7895, 1990.

[34] J. K. Burdett, T. Hughbanks, G. J. Miller, J. W. Richardson, and J. V. Smith, "Structural-electronic relationships in inorganic solids: powder neutron diffraction studies of the rutile and anatase polymorphs of titanium dioxide at 15 and 295 K," *Journal of the American Chemical Society*, vol. 109, no. 12, pp. 3639–3646, 1987.

[35] J. Sato, H. Kobayashi, and Y. Inoue, "Photocatalytic activity for water decomposition of indates with octahedrally coordinated d10 configuration. II. Roles of geometric and electronic structures," *Journal of Physical Chemistry B*, vol. 107, no. 31, pp. 7970–7975, 2003.

[36] J. P. Perdew and M. Levy, "Physical content of the exact kohn-sham orbital energies: band gaps and derivative discontinuities," *Physical Review Letters*, vol. 51, no. 20, pp. 1884–1887, 1983.